A R C H I V E O F M E C H A N I C A L E N G I N E E R I N G

Volume 68 2021 Number 4

DOI: 10.24425/ame.2021.139312

Key words: underwater manipulator, drag, added inertia, motion planning, recursive Lagrangian formulation, redundant manipulator, obstacle avoidance, singularity avoidance

Virendra Kumar [1], Soumen Sen [1], Shibendu Shekhar Roy [2]

Motion planning of planar and redundant underwater serial link manipulator based on minimization of energy consumption

The article describes motion planning of an underwater redundant manipulator with revolute joints moving in a plane under gravity and in the presence of obstacles. The proposed motion planning algorithm is based on minimization of the total energy in overcoming the hydrodynamic as well as dynamic forces acting on the manipulator while moving underwater and at the same time, avoiding both singularities and obstacle. The obstacle is considered as a point object. A recursive Lagrangian dynamics algorithm is formulated for the planar geometry to evaluate joint torques during the motion of serial link redundant manipulator fully submerged underwater. In turn the energy consumed in following a task trajectory is computed. The presence of redundancy in joint space of the manipulator facilitates selecting the optimal sequence of configurations as well as the required joint motion rates with minimum energy consumed among all possible configurations and rates. The effectiveness of the proposed motion planning algorithm is shown by applying it on a 3 degrees-of-freedom planar redundant manipulator fully submerged underwater and avoiding a point obstacle. The results establish that energy spent against overcoming loading resulted from hydrodynamic interactions majorly decides the optimal trajectory to follow in accomplishing an underwater task.

1. Introduction

The two-third of the earth's surface is covered by the sea, and an abundant amount of resources are preserved within it. To recover these resources, undersea exploration has become important in recent years. Recovery of materials/resources

✉ Virendra Kumar, e-mail: vkumar@cmeri.res.in

[1]Robotics and Automation Division, CSIR-Central Mechanical Engineering Research Institute, Durgapur, India. ORCID V.K.: 0000-0002-2762-4249

[2]Mechanical Engineering Department, National Institute of Technology, Durgapur, India.

from inaccessible underwater environment, underwater robots like the autonomous underwater vehicles (AUVs), and remotely operated vehicles (ROVs) equipped with underwater manipulators are employed. Few other applications as well include material handling and rescue, pipeline maintenance and welding of underwater structure, underwater operations etc. For the complex applications in many cases, manipulators require to have joint-space redundancy to reach complex or narrow areas. One of the most important aspects of the underwater manipulator operation is to plan trajectories such that energy demand is minimized, because the energy available in underwater vehicle manipulator system is limited. This article presents such a motion planning approach for planar underwater manipulator with joint-space redundancy in order to minimize energy consumption.

Literature presents several approaches to resolve redundancy in motion planning of the serial-link redundant manipulator and various mathematical tools are available for that. Moore-Penrose Generalized Inverse [1] is a commonly used tool. Motion planning of serial link redundant manipulators considering different kinematic and dynamic criteria such as torque optimization, time minimization, obstacle avoidance, energy optimization, and other objective functions are proposed in the literature [2–4]. Authors of [2] presented a method considering the manipulator dynamic for a time-optimal motion planning. Authors of [3] proposed a trajectory planning method that satisfies the dynamic equations of the system. Authors of [4] developed a jerk-bounded trajectory for an industrial robot.

Available literature sparsely considered motion/trajectory planning of underwater robotic systems [5–8]. Ref. [5] used a pseudoinverse method to resolve the task priority based redundancy for an autonomous Underwater Vehicle-Manipulator System (UVMS) by using a kinematic approach. For an underwater robotic vehicle system, authors of [6] presented a robust trajectory control approach for redundancy resolution. Authors of [7] described genetic algorithm (GA) based planning for finding a safe path with minimized energy cost in presence of strong currents and proposed the method to avoid getting trapped by local minima. Authors of [8] presented a coordinated motion planning algorithm for autonomous underwater vehicle manipulator system to minimize the hydrodynamic drag force acting on the system.

For dynamic based trajectory planning, the study of dynamics of underwater manipulators is needed; however literature presents a limited discussion on this [9–11]. Among them, majority described the hydrodynamic modelling in rigid body frame work using empirical formulations. Hydrodynamic modelling expressed in literature is characterized by three dominant effects namely, inertial effect, hydrodynamic drag and buoyancy [9–12]. In the fluid mechanics literature the standard empirical expressions for the hydrodynamic forces are available which are used by different researchers for underwater manipulator modelling [10, 13]. Among the hydrodynamic drags forces, the most dominant component, i.e. the pressure drag is discussed in [10] for application in underwater manipulator. The other non-dominant/negligible component of the hydrodynamic drag forces such as the skin

friction drag, is not generally considered in the formulation. The hydrodynamic forces (drag force and added mass/inertia forces) are function of the instantaneous configuration of the underwater manipulator. In most of the above mentioned literatures, the dynamic algorithms are either based on Newton Euler (NE) or on Lagrange-Euler (LE) approach. Exceptionally, authors of [13] applied Kane's method in deriving the dynamics for underwater manipulator.

This article considers trajectory planning of a stationary-base planar underwater manipulator with revolute joints based on minimization of the total energy in overcoming dynamic and hydrodynamic forces in underwater scenario. During the motion planning, obstacle and singularity avoidances are also considered. Here, a new approach for computation of dynamics of underwater planar manipulator is developed based on a recursive Lagrangian formulation and then used for performing the underwater motion planning. The derivation of dynamics algorithm was motivated by the recursive Lagrangian method proposed in [14] for aerial manipulator. The formulation is used for the torque and power calculation during trajectory planning. Empirical formulations found in standard literature [11, 12, 15] are employed for pressure drag and added mass computations for the moving links of the manipulator. Eventually an algorithm is presented here that generates the desired trajectory of the redundant underwater manipulator with revolute joints such that total energy of operation is minimized and the manipulator steer clears a point obstacle present within workspace and in the same time keeps distance from occurrence of possible singularities. In majority of practical scenarios, redundancy is present in a single plane, while in spatial applications, other planes do not generally contain redundant motions. This article primarily emphasizes on establishing the principle of energy optimum motion planning for redundant underwater manipulators. Hence, to avoid complexities of spatial mechanisms, a planar problem is chosen here, which adequately address the said principle of motion planning of underwater manipulator.

The next section describes the definitions of different hydrodynamic forces acting on manipulators. Then, it presents the recursive Lagrangian dynamics algorithm, followed by the principles of obstacle and singularity avoidance. Then, the proposed trajectory planning algorithm is formulated and presented. In the last section, simulation of a case study of a planar three degrees of freedom manipulator is presented and discussed. The article is then concluded stating effectiveness of the proposed method and the future work being taken up.

2. Hydrodynamic forces on links

In the present analysis, hydrodynamic forces of interaction are modelled in the rigid body mechanics framework based on empirical formulation found in the literatures. The hydrodynamic added mass/inertia force, hydrodynamic drag force and buoyancy force are found to be the main contributor to the net hydrodynamic

effect. In the following, the definitions of these force components are stated briefly. Throughout the paper, the words 'fluid' and 'water' are synonymously used.

2.1. Drag force

When a body moves within a fluid (fully or partially submerged) it experiences dissipative resistances, which are generally called hydrodynamic drag. The dominating component of the net drag force comes from pressure drag and other drag forces are usually neglected (see [10]). The hydrodynamic drag force is a function of link joint angles, link geometry, drag coefficients, density of fluid and relative link velocities with respect to fluid and expressed as in Eq. (1).

$$\mathbf{f}_d = -0.5\rho\, C_d A \,\|\mathbf{v}^n\|\, \mathbf{v}^n, \tag{1}$$

where A represent the projected area of the link geometry normal to the velocity, $\mathbf{v}^n$ is the normal velocity component in base frame, C_d is the drag coefficient, ρ is the density of water. The drag coefficient value for different types of standard geometry and flow conditions can be found in [14] and appropriately chosen in the present formulation. The negative sign indicates the direction of drag being opposite to velocity direction.

2.2. Added mass

When a body (such as a link of the underwater manipulator) is accelerated or decelerated within a fluid medium, that causes a certain amount of surrounding fluid also to be accelerated or decelerated along with the body. The force, responsible to accelerate/decelerate the surrounding fluid generates a reaction force on the object, opposite to the direction of motion of the object or link. This opposite force acting on the accelerating/decelerating body due to the fluid interaction is known as added mass/inertia force. The added mass forces and moments are derived by applying potential theory. Here, assumptions are made that fluid is inviscid, irrotational and incompressible [15]. The force/moment being proportional to the mass/inertia of the surrounding fluid causes an increase in perceived effective mass/inertia of the moving submerged body. This additional inertia component is known as Added Mass or Added Inertia. The added mass also contributes to added Coriolis and centripetal forces. Formulation for computing the added mass/inertia of bodies of common shape and sizes are available in standard literature [11, 15].

For a cylindrical rigid body of mass m_i diameter d_i and length L_i, in planar application where gravitational force acting in Y-axis and Z-axis is out of plane, the empirically derived added mass coefficients are represented as follows:

$$\mathbf{M}_A = -\mathrm{diag}\,\{X_{\dot{u}},\, Y_{\dot{v}},\, N_{\dot{r}}\}, \tag{2}$$

where, $X_{\dot{u}} = -0.05m_i$; $Y_{\dot{v}} = -\pi\rho(d_i/2)^2 L_i$; $N_{\dot{r}} = -\pi\rho(d_i/2)^2 L_i^3/12$ and $\mathbf{M}_A \in \mathbb{R}^{3\times 3}$.

$X_{\dot{u}}$ is the added mass coefficient along the length of the link, according to the chosen body-fixed frame. The above empirical expressions (for practical applications) are obtained from the generalized derivation for spatial underwater case in [11, 15].

2.3. Restoring forces

A submerged body in a fluid experiences two other dominant forces, namely gravity and buoyancy force. They are commonly named as restoring forces. The buoyancy force is due to the hydrostatic effect, i.e., it is independent of the relative movement between the fluid and body. These forces act at the centre of buoyancy of the body, which is equivalently the centre of mass of fluid displaced by the body. The weight W and buoyancy force B are expressed in the body-fixed frame by

$$\begin{aligned} \mathbf{f}_g &= -{}^{i}\mathbf{R}_0 \begin{bmatrix} 0 \\ W \end{bmatrix}, \\ \mathbf{f}_B &= {}^{i}\mathbf{R}_0 \begin{bmatrix} 0 \\ B \end{bmatrix}, \end{aligned} \tag{3}$$

where ${}^{i}\mathbf{R}_0$ is the planar rotation matrix from base frame $\{0\}$ to the link frame $\{i\}$ of the i-th link.

3. Recursive Lagrangian dynamics

Using total kinetic energy $\mathcal{K}$ and total potential energy $\mathcal{P}$ of the system, the functional Lagrangian $\mathcal{L}$ is formed:

$$\mathcal{L} = \mathcal{K} - \mathcal{P} \,. \tag{4}$$

The joint angles of the serial link manipulator $\mathbf{q}_i$, where $\mathbf{q}_i$ is the i-th element of the vector $\mathbf{q} \in \mathbb{R}^n$, are chosen as the generalized coordinates.

For an underwater manipulator system, the total kinetic energy is the summation of the kinetic energy of manipulator and kinetic energy of moving surrounding water. Drag force present in the system is of dissipative in nature, and the consideration of all velocity dependent dissipative forces in the system is solved using Raleigh Dissipation Potential function. Hence the dynamic model for underwater moving body system based on Lagrange–Euler formulation is obtained as Eq. (5) in the below.

$$\frac{\mathrm{d}}{\mathrm{d}t}\left(\frac{\partial \mathcal{L}}{\partial \dot{\mathbf{q}}_i}\right) - \frac{\partial \mathcal{L}}{\partial \mathbf{q}_i} + \frac{\partial \mathcal{F}}{\partial \dot{\mathbf{q}}_i} = \boldsymbol{\tau}_i \,; \quad i = 1, \ldots, n, \tag{5}$$

where, $\boldsymbol{\tau}_i$ are the generalized forces and $\mathbf{q}_i$ are the generalized coordinates to describe the configuration and $\mathcal{F}$ is a Raleigh Dissipation function, such that $\dfrac{\partial \mathcal{F}}{\partial \dot{\mathbf{q}}_i}$

represents the velocity dependent drag force. Buoyancy force term is included along with the gravity force in the total potential energy term $\mathcal{P}$.

Fig. 1 describes the geometry and nomenclature for link-i of the manipulator describing the different parameters of the link. The frame $\{i\}$ on the link-i is attached at the distal end of the link. $\mathbf{c}_i$ is the centre of mass of link-i, $\bar{\mathbf{r}}_i \in \mathbb{R}^2$ is position of centre of mass and $\mathbf{p}_i \in \mathbb{R}^2$ is the position of the frame $\{i\}$, all expressed in base frame. For ease of description using conventional notation, the link geometries are shown in a 3-D space in Fig. 1.

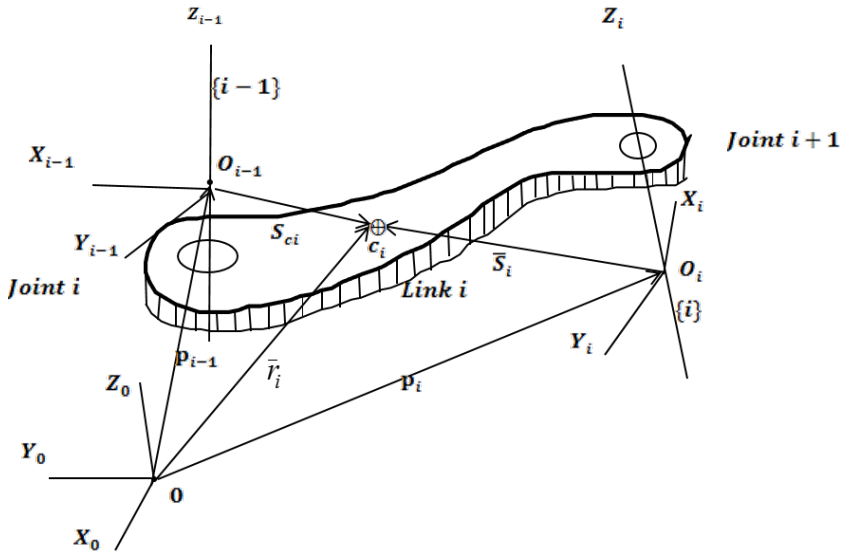

Fig. 1. Representation of link-i, which rotates on joint-i. Joint-i connects link-$(i-1)$ and link-i. Frame-i is located on the axis of joint $(i+1)$

The torques on each joint are evaluated using recursive Lagrangian formulation. The velocities are computed in the forward recursion, while the forces/torques are estimated in the backward recursion [16]. Thus, for the n link completely submerged manipulator, the Lagrangian $\mathcal{L}$ is defined as

$$\mathcal{L} = \sum_{i=1}^{n} \mathrm{tr}\left(\frac{1}{2}\mathbf{M}_i \mathbf{V}_i \mathbf{V}_i^T\right) - \sum_{i=1}^{n} \mathcal{P}_i\,, \tag{6}$$

where, $\mathbf{V}_i = \begin{bmatrix} \mathbf{v}_i \\ \boldsymbol{\omega}_i \end{bmatrix} \in \mathbb{R}^3$; $\mathbf{v}_i \in \mathbb{R}^2$ is the linear velocity in $x-y$ plane and $\boldsymbol{\omega}_i \in \mathbb{R}^1$ is the angular velocity about Z_{i-1} axis of link-i in base frame.

$\mathbf{M}_i = \mathbf{M}_{Ri} + \mathbf{M}_{Ai}$; $\mathbf{M}_{Ri}$ and $\mathbf{M}_{Ai}$ are rigid body and added mass inertia matrices respectively. For the planar case, all of $\mathbf{M}_{Ri},\ \mathbf{M}_{Ai} \in \mathbb{R}^{3\times 3}$.

The equations of motion are thus derived using the Euler-Lagrange formulation, as described in the following.

$$\frac{\mathrm{d}}{\mathrm{d}t}\left(\frac{\partial \mathcal{L}}{\partial \dot{\mathbf{q}}_i}\right) = \sum_{j=i}^{n} \mathrm{tr}\frac{1}{2}\left[\mathbf{M}_j \frac{\mathrm{d}}{\mathrm{d}t}\left(\frac{\partial(\mathbf{V}_j)}{\partial \dot{\mathbf{q}}_i}\right)\mathbf{V}_j{}^T + \mathbf{M}_j \frac{\partial \mathbf{V}_j}{\partial \dot{\mathbf{q}}_i}\frac{\mathrm{d}(\mathbf{V}_j{}^T)}{\mathrm{d}t} + \mathbf{M}_j \frac{\mathrm{d}(\mathbf{V}_j)}{\mathrm{d}t}\frac{\partial \mathbf{V}_j{}^T}{\partial \dot{\mathbf{q}}_i} + \mathbf{M}_j \mathbf{V}_j \frac{\mathrm{d}}{\mathrm{d}t}\left(\frac{\partial(\mathbf{V}_j)}{\partial \dot{\mathbf{q}}_i}\right)\right] \tag{7}$$

and

$$\frac{\partial \mathcal{L}}{\partial \mathbf{q}_i} = \sum_{j=i}^{n} \mathrm{tr}\frac{1}{2}\left[\mathbf{M}_j \frac{\partial \mathbf{V}_j}{\partial \mathbf{q}_i}\mathbf{V}_j{}^T + M_j V_j \frac{\partial \mathbf{V}_j{}^T}{\partial \mathbf{q}_i}\right] - \sum_{j=i}^{n}\left(m_j - \rho \mathcal{V}_j\right)\mathbf{g}^T \frac{\partial(\mathbf{P}_{j-1} + {}^0\mathbf{R}_j\, {}^j\mathbf{s}_{cj})}{\partial \mathbf{q}_i}, \tag{8}$$

where $\mathbf{g}$ is gravitational force.

Using the following properties (see derivation in [16])

(i) $\dfrac{\partial \mathbf{V}_j}{\partial \mathbf{q}_i} = \dfrac{\mathrm{d}}{\mathrm{d}t}\left(\dfrac{\partial \mathbf{V}_j}{\partial \dot{\mathbf{q}}_i}\right)$ (for the present planar case) and

(ii) $\mathrm{tr}\left(\mathbf{A}\,\mathbf{B}^T\right) = \mathrm{tr}\left(\mathbf{B}\,\mathbf{A}^T\right)$, where $\mathbf{A},\ \mathbf{B} \in \mathbb{R}^{3\times 3}$ are two matrices)

and on rearranging the terms, the total joint torque for joint-i is obtained as

$$\boldsymbol{\tau}_i = \sum_{j=i}^{n} \mathrm{tr}\left[\frac{\partial \mathbf{V}_j}{\partial \dot{\mathbf{q}}_i}\frac{\mathrm{d}(\mathbf{V}_j^T)}{\mathrm{d}t}\mathbf{M}_j\right] - \mathbf{g}^T \sum_{j=i}^{n}\left(m_j - \rho \mathcal{V}_j\right)\frac{\partial\left(\mathbf{P}_{j-1} + {}^0\mathbf{R}_{j-1}\, {}^{j-1}\mathbf{S}_{cj}\right)}{\partial q_i} + \frac{\partial \mathcal{F}_i}{\partial \dot{\mathbf{q}}_i}. \tag{9}$$

The last term in Eq. (9) is the torque due to drag forces on link-i, $\boldsymbol{\tau}_{di} = \dfrac{\partial \mathcal{F}_i}{\partial \dot{\mathbf{q}}_i}$ evaluated from the velocity dependent *Rayleigh* dissipation function, $\mathcal{F}_i$.

The net joint torque at joint $i(= l)$ due to drag forces is contributed by the torques due to drag forces experienced by all the links beyond for $i = l$ to n. Thus, at joint $i(= l)$, the net dissipation energy due to all links ($i = l$ to n) is represented by $\mathcal{F}_l = \dfrac{1}{3}\sum_{i=l}^{n} C_i v_{ci}^3$, where, v_{ci} is the normal velocity component on the link-i expressed in base the frame and $C_i = \dfrac{1}{2}\rho C_{di} A_i$. A_i is the projected area and C_{di} is the drag coefficient for the i-th link. Values of C_{di} for some regular geometries are available in literature (such as [12, 15]).

For a link ($i = l$), evaluating the centre of drag point [17] and expressing J_{dl} as the Jacobian at the centre of drag point, joint torque due to drag forces, τ_{dl} can be arranged as

$$\begin{aligned} \boldsymbol{\tau}_{dl} &= \sum_{i=l}^{n} C_i \mathbf{v}_{ci}^2 \frac{\partial \mathbf{v}_{ci}}{\partial \dot{\mathbf{q}}_i} = \sum_{i=l}^{n} \frac{1}{2} \rho\, C_{di} A_i \mathbf{v}_{ci}^2 \frac{\partial \mathbf{v}_{ci}}{\partial \dot{\mathbf{q}}_i} \quad \text{or} \\ \boldsymbol{\tau}_{dl} &= [\mathbf{a}_{1\times l}]_l \, \mathbf{J}_{dl}{}^T \mathbf{f}_{dl} + \sum_{j=l+1}^{n} \left[\mathbf{a}_{1\times j}\right]_l \mathbf{J}_{dj}{}^T \mathbf{f}_{dj} \end{aligned} \tag{10}$$

where $\mathbf{f}_{di} = C_i \mathbf{v}_{ci}^2$ represents the resultant drag force on link-i, $\mathbf{J}_{di} \in \mathbb{R}^{2\times n}$ is an $2 \times n$ dimensional matrix for planar manipulator.

$[\mathbf{a}_{1\times j}]_l \in \mathbb{R}^{1\times j}$ denotes a j-dimensional row vector with 1 in the l-th entry and rest of the elements equal 0 [16]. i and j are the indices, varying from 1 to n.

The gravity and buoyancy related term,

$$\mathbf{g}^T \sum_{j=i}^{n} \left(m_j - \rho \mathcal{V}_j\right) \frac{\partial \left(\mathbf{P}_{j-1} + {}^0\mathbf{R}_{j-1}\, {}^{j-1}\mathbf{S}_{cj}\right)}{\partial \mathbf{q}_i}$$

can be rearranged and written in a recursive form as $\mathbf{g}^T \dfrac{\partial \beta_i}{\mathrm{d}\mathbf{q}_i}$, where,

$$\beta_i = (m_i - \rho \mathcal{V}_i)\, {}^0\mathbf{R}_{i-1}\, {}^{i-1}\mathbf{s}_{ci} + (m_{i+1} - \rho \mathcal{V}_{i+1})\, \mathbf{P}_i + \beta_{i+1},$$

$\mathcal{V}_i$ is the displaced water volume due to link$-i$, m_i is the mass of link-i and ${}^{i-1}\mathbf{s}_{ci} \in \mathbb{R}^2$ is the position vector of the centre of mass of link-i in frame $i-1$.

The iteration for torque computations starts from $i = n$, moves backward and terminates after $i = 1$.

A $t = n$, $\beta_n = (m_n - \rho \mathcal{V}_n)\, {}^0\mathbf{R}_{n-1}\, {}^{n-1}\mathbf{s}_{cn}$, having $m_{i+1} = 0$, $\mathcal{V}_{i+1} = 0$, and $\beta_{i+1} = 0$. Again at $i = 1$, $\beta_1 = (m_1 - \rho \mathcal{V}_1)\, {}^0\mathbf{R}_0\, {}^0\mathbf{s}_{c1} + (m_2 - \rho \mathcal{V}_2)\, \mathbf{P}_1 + \beta_2$.

The entire computation for the joint torques can be structured in a recursive fashion as in the following algorithm.

The algorithm first computes the velocities in the forward recursion, followed by torque computation in the backward recursion.

Forward Recursion:

$$\begin{bmatrix} \mathbf{v}_{i+1} \\ \boldsymbol{\omega}_{i+1} \end{bmatrix} = \begin{bmatrix} 1 & 0 & K_{i,i+1\_y} \\ 0 & 1 & -K_{i,i+1\_x} \\ 0 & 0 & 1 \end{bmatrix} \begin{bmatrix} \mathbf{v}_i \\ \boldsymbol{\omega}_i \end{bmatrix} + [\check{\mathbf{e}}_{i+1} + \tilde{\mathbf{z}}_{i+1}]\, \dot{\mathbf{q}}_{i+1},$$

$$V_{i+1} = \mathbf{D}_{i,i+1} V_i + [\check{e}_{i+1} + \tilde{z}_{i+1}]\, \dot{q}_{i+1},$$

where

$\mathbf{v}_{i+1} \in \mathbb{R}^2$ and $\boldsymbol{\omega}_{i+1} \in \mathbb{R}^1$,

$\dot{\mathbf{q}}_{i+1}$ is the joint rate of joint-$(i+1)$,

$\bar{\mathbf{s}}_i$ is the vector from the centre of mass of the i-th link to the $(i+1)$-th joint,

$\mathbf{s}_{ci}$ is the vector from i-th joint to the centre of mass of the i-th link (see Fig. 1),

$\bar{\mathbf{s}}_i + \mathbf{s}_{c\,i+1} = \mathbf{K}_{i,i+1}$,

$$\mathbf{D}_{i,i+1} = \begin{bmatrix} 1 & 0 & K_{i,i+1\_y} \\ 0 & 1 & -K_{i,i+1\_x} \\ 0 & 0 & 1 \end{bmatrix},$$

$K_{i,i+1\_x}$ and $K_{i,i+1\_y}$ are the x and y components of the position vector $\mathbf{K}_{i,i+1}$.

$\check{\mathbf{e}}_{i+1} = \tilde{\mathbf{z}}_{i+1} \times \begin{bmatrix} \mathbf{s}_{c\,i+1} \\ 0 \end{bmatrix}$ (cross product of the two vectors results into the vector representing velocity direction at centre of mass of the $(i+1)$-th link due to angular motion at joint $(i+1)$), and $\tilde{\mathbf{z}}_{i+1} = [0 \;\; 0 \;\; 1]^T$ is the unit vector along the axis of rotation of the $(i+1)$-th joint, which is normal to the plane of motion.

Backward recursion:

$$\boldsymbol{\tau}_i = \mathrm{tr}\left[\frac{\partial \mathbf{V}_i}{\partial \dot{\mathbf{q}}_i}\boldsymbol{\mathcal{B}}_i\right] + \sum_{j=i+1}^{n} \mathrm{tr}\left[\frac{\partial \mathbf{V}_j}{\partial \dot{\mathbf{q}}_i}\boldsymbol{\mathcal{B}}_j\right] - \mathbf{g}^T \frac{\partial \beta_i}{\partial \mathbf{q}_i} + \boldsymbol{\tau}_{di},$$

where, $\boldsymbol{\mathcal{B}}_i = \dfrac{\mathrm{d}(\mathbf{V}_i{}^T)}{\mathrm{d}t}\mathbf{M}_i$

and

$$\boldsymbol{\tau}_{di} = [\mathbf{a}_{1\times i}]_i \, \mathbf{J}_{di}{}^T \mathbf{f}_{di} + \sum_{j=i+1}^{n} \left[\mathbf{a}_{1\times j}\right]_i \mathbf{J}_{dj}{}^T \mathbf{f}_{dj}.$$

At each step of forward recursion, velocity is evaluated and term $\boldsymbol{\tau}_i$ is calculated in backward recursion using $\boldsymbol{\mathcal{B}}_i$, β_i and $\mathbf{f}_{di}$ from link $i = n$ to 1. $\boldsymbol{\mathcal{B}}_i$, β_i and $\mathbf{f}_{di}$ are computed in the backward direction from link $i = n$ to 1 and their computations are terminated when $i = 0$. For $i > n$, there exists no link and β_i, $\boldsymbol{\mathcal{B}}_i$ and $\mathbf{f}_{di}$ become zero.

4. Obstacle and singularity avoidance

Obstacle avoidance becomes necessary in presence of any obstacle within the workspace of the manipulator while completing a motion task. Obstacle avoidance is activated when there a possibility of collision with obstacles is identified. This additional task is used for redundancy resolution and solved by using configuration control. To derive the obstacle avoidance algorithm, three processes are needed [18]. First, the critical point on the links (location of the possible point of the collision on the link) is identified and distances of the critical point to the obstacles are calculated at every instant of time. In the second step a decision is taken based

on the distance of links to the obstacle to determine if the additional task of obstacle avoidance should be activated for the link or not. The third step applies configuration control for redundancy resolution to find joints rates in avoiding the obstacle. Fig. 2 shows the link-i and obstacle-j model and their positions and the location of the critical point. The critical distance h_{ij} between link-i and obstacle-j is obtained as in Fig. 2 as

$$h_{ij} = \left\| \mathbf{h}_i - \mathbf{p}_j \right\|, \tag{11}$$

where $\mathbf{h}_i$ is the position vector of the critical point (H_i) on link-i, which is obtained by projection of obstacle on the link. As shown in Fig. 2, the critical point (H_i) may also be below the point B_i or above T_i, depending on the position of the obstacle and accordingly B_i or T_i will become a critical point.

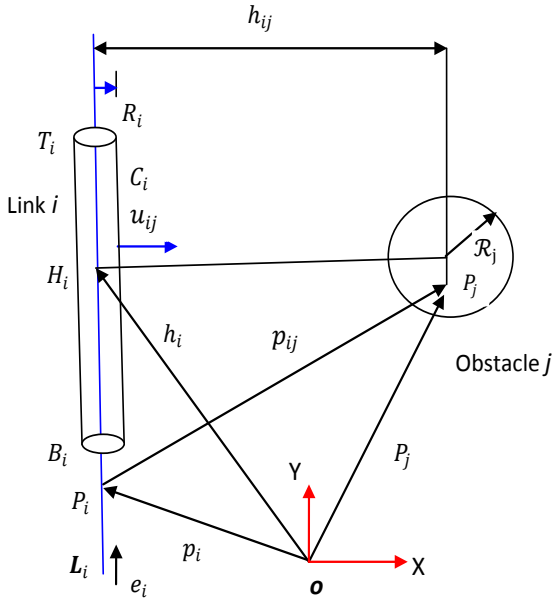

Fig. 2. Collision detection between link-i and object-j

Singularity avoidance is incorporated by taking an approach that joint velocity should not attain an extremely high velocity. Singularity avoidance is mathematically expressed such that the manipulator end-effector Jacobian does not become ill-conditioned. Thus for obstacle avoidance for each link-i the second criterion (additional task) is expressed as a function

$$\mathbf{z}_i = f_i\left(\mathbf{q}, t\right) = \mathcal{R}_j - h_{ij}\,, \tag{12}$$

where $\mathcal{R}_j$ is the radius of a circular safe region made around the obstacle centre. The secondary criterion of the obstacle avoidance guarantees that the links steer

clear of the safe region. The secondary tasks' desired rate is zero on the boundary of the safety region and expresses as Eq. (13).

$$\dot{\mathbf{z}}_i^d = 0. \tag{13}$$

Now if $\mathbf{x}$ is the coordinate of the end effector in task space, then the primary task of reachability of the manipulator as well as the secondary task or additional task described by $\dot{\mathbf{z}}$ are required to be satisfied.

$$\mathbf{x} = f(\mathbf{q}), \tag{14}$$

$$\dot{\mathbf{x}} = \mathbf{J}_e \dot{\mathbf{q}}, \tag{15}$$

$$\dot{\mathbf{z}} = \mathbf{J}_c \dot{\mathbf{q}}. \tag{16}$$

If $\dot{\mathbf{x}}^d$ and $\dot{\mathbf{z}}^d$ represent the desired velocities of the main task and additional task respectively, then the joint velocity $\dot{\mathbf{q}}$ are evaluated in such a way that the primary main task errors and secondary tasks errors are minimized. In the formulation of the cost function, the singularity avoidance is taken care by penalizing high joint rates. Applying the configuration control method the composite cost function to be minimized is formulated [18] as below

$$F = \left(\mathbf{J}_e \dot{\mathbf{q}} - \dot{\mathbf{x}}^d\right)^T \mathbf{W}_e \left(\mathbf{J}_e \dot{\mathbf{q}} - \dot{\mathbf{x}}^d\right) + \dot{\mathbf{q}}^T \mathbf{W}_v \dot{\mathbf{q}} + \left(\mathbf{J}_c \dot{\mathbf{q}} - \dot{\mathbf{z}}^d\right)^T \mathbf{W}_c \left(\mathbf{J}_c \dot{\mathbf{q}} - \dot{\mathbf{z}}^d\right), \tag{17}$$

where, $\mathbf{W}_e$, $\mathbf{W}_c$, and $\mathbf{W}_v$ are positive definite weighting matrix with appropriate matrix dimensions. After the minimization of the above function F the joint rates are evaluated as

$$\dot{\mathbf{q}} = \left(\mathbf{J}_e{}^T \mathbf{W}_e \mathbf{J}_e + \mathbf{J}_c{}^T \mathbf{W}_c \mathbf{J}_c + \mathbf{W}_v\right)^{-1} \left(\mathbf{J}_e{}^T \mathbf{W}_e \dot{\mathbf{x}}^d + \mathbf{J}_c{}^T \mathbf{W}_c \dot{\mathbf{z}}^d\right). \tag{18}$$

5. Optimization formulation and evaluation

The optimization problem is formulated for the trajectory tracking motion planning with minimum energy to overcome the dynamic and hydrodynamic forces of interaction acting on the links while avoiding an obstacle as well as singularity configurations. The solution for redundancy resolution is obtained by choosing only those configurations which minimize energy against all the dynamic and hydrodynamic effects under given constraints of manipulator end effect or reachability, and avoidance of singularity and obstacle. By using the recursive Lagrangian algorithm the joint torques, $\boldsymbol{\tau}_i$ are calculated, and instantaneous dynamic power can be evaluated as in the below:

$$P(\mathbf{q}, \dot{\mathbf{q}}, \ddot{\mathbf{q}}, t) = \sum_{i=1}^{n} |\boldsymbol{\tau}_i| \, |\dot{\mathbf{q}}_i|, \tag{19}$$

where P is the power which is function of joint angles, joint angular velocities and joint angular accelerations. The motion planning task for n degree-of-freedom manipulator is then formulated as a constrained optimization problem using Eq. (14) and Eq. (18). Objective is to minimize the total energy in accomplishing the desired task with specified reachability and end motion conditions.

$$\min_{\mathbf{q}} \int_{t_0}^{t_f} P\left(\mathbf{q},\, \dot{\mathbf{q}},\, \ddot{\mathbf{q}}, t\right) \mathrm{d}t$$

Subject to

$$\begin{aligned} \mathbf{x} &= f\left(\mathbf{q}(t)\right), \\ \dot{\mathbf{q}}(t) &= \left(\mathbf{J}_e{}^T \mathbf{W}_e \mathbf{J}_e + \mathbf{J}_c{}^T \mathbf{W}_c \mathbf{J}_c + \mathbf{W}_v\right)^{-1} \mathbf{J}_e{}^T \mathbf{W}_e \dot{\mathbf{x}}, \\ \mathbf{q}_{il} &< \mathbf{q}_i < \mathbf{q}_{iu}, \end{aligned}$$

where, $i = 1$ to n.

The optimization procedure is described as in the below.

1. Define a trajectory from position $\mathbf{x}_1$ to $\mathbf{x}_{N+1} = \mathbf{x}^d$ with N intervals in time T seconds.
2. Find the inverse kinematic for initial position $\mathbf{x}_1$ assuming the angle of initial posture $\mathbf{q}_1$.
3. Calculate the end effector velocity $\dot{\mathbf{x}}_k$ at the time instant k.
4. Find the joint rates $\dot{\mathbf{q}}_k$ using Eq. (18) considering the singularity and obstacle avoidance algorithm as
   (a) $\dot{\mathbf{q}}_k = \left(\mathbf{J}_e{}^T \mathbf{W}_e \mathbf{J}_e + \mathbf{J}_c{}^T \mathbf{W}_c \mathbf{J}_c + \mathbf{W}_v\right)^{-1} \left(\mathbf{J}_e{}^T \mathbf{W}_e \dot{\mathbf{x}}_k^d + \mathbf{J}_c{}^T \mathbf{W}_c \dot{\mathbf{z}}_k^d\right)$
5. Evaluate the forces and torques
6. Repeat step (2) to (5) for $k = 1, \ldots, N$
7. Evaluate total energy and store
8. Change the initial posture by small angle $\Delta\mathbf{q}_1$ and repeat step (2) to (8) until $\mathbf{q}_1$ reaches the maximum joint range angle.
9. Find minimum energy and corresponding manipulator configurations.

In this article, a serial link manipulator with only revolute joints is considered for the motion planning. A planar exemplar demonstration through simulation is chosen for ease of computation, since the objective of this article is to establish the principle of the proposed underwater motion planning. The recursive Lagrangian algorithm (formulated for planar application only) is used to compute the inverse dynamics (due to dynamic and hydrodynamic loading) of the manipulator, which is used for determination of joint torques ($\boldsymbol{\tau}$) for instantaneous power evaluation in Eq. (19). The optimization process gives the output trajectories in joint space while the end effector of the manipulator follow a path in the Cartesian task space defined by Eq. (14).

6. Simulation: Result and discussion

The optimization method described in previous section is applied on a 3 degrees-of-freedom (DOF) planar underwater manipulator moving in a vertical plane against the gravity in fully submerged condition. The links of the underwater manipulator are assumed as right circular cylindrical objects with link-lengths 0.5 m, 0.4 m and 0.3 m respectively, link diameters being 0.080 m. The manipulator links are approximately neutrally buoyant with the mass of links taken as 2.5 kg, 2.0 kg and 1.5 kg respectively. It is assumed that the end effector of the underwater manipulator follows a straight-line path in the task space, from a starting point (0.50 m, 0.80 m) to a goal point (−0.30 m, 0.6 m) with initial and final velocity as zero and in time of 1 second following a cubic polynomial in the task space trajectory. The gravity acts in negative y-direction and buoyancy in the positive y-direction and both act at the centre of mass of each link. In simulation environment, obstacle is assumed as a point object and is kept at (0.0 m, 0.30 m) and radius of safe circle region is taken as 0.05 m. Simulations are carried out in Matlab®(from MathWorks Inc.). The results are plotted and described in the Figs. 3 to 16. The series of manipulator configurations corresponding to the minimum total energy consumed against overcoming the underwater forces (dynamic and hydrodynamic) is shown in Fig. 3.

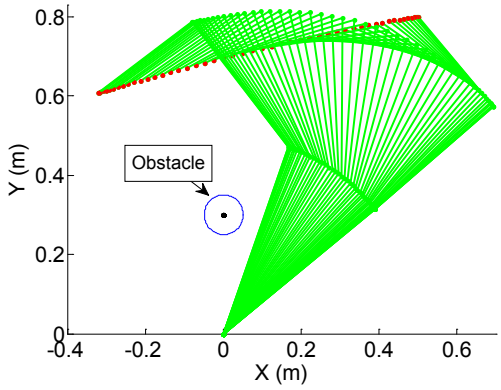

Fig. 3. Series of manipulator configurations corresponding to minimum total energy while the end effector follows a Cartesian straight line path and avoiding obstacle and singularity

Fig. 4 shows the instantaneous total power requirement corresponding to total minimum-energy motions against various non-optimal motions during the Cartesian straight line path following. The red solid line represents the power curve for minimum energy motion tracking and the rest green lines represent the power curve corresponding to non-optimal energy motion tracking. The optimal configurations (joint angles) and joint rates are reported in Fig. 5 and Fig. 6, respectively.

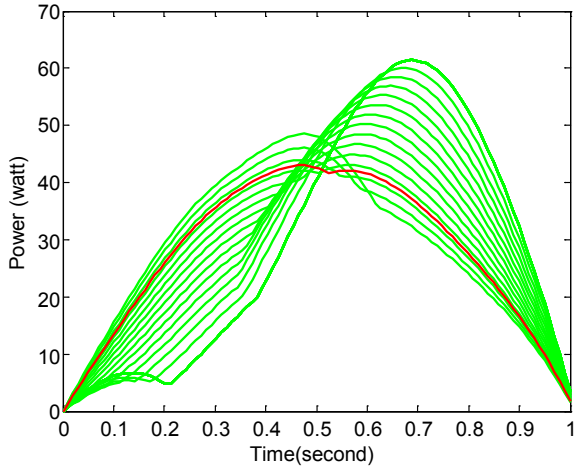

Fig. 4. Simulation results for instantaneous total power requirement during the Cartesian straight line path following. The solid red line shows power corresponding to the minimum energy motion while solid green lines represent non-optimal motions

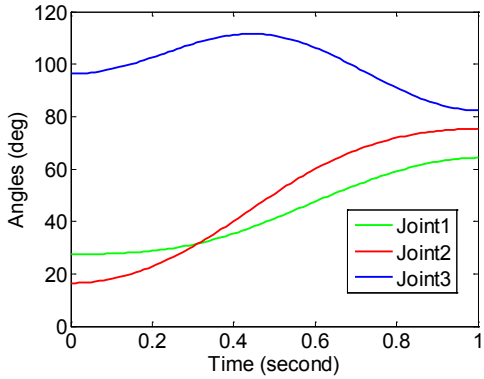

Fig. 5. Joint angles corresponding to minimum energy motion planning

Similarly, torque on joints corresponding to minimum energy motion is shown in Fig. 7.

The drag forces and their directions on the links corresponding to minimum energy configurations are shown in Fig. 8 and Fig. 9. These two figures show instantaneous configurations at time instances of 0.4 s and 0.5 s respectively, where, the change in drag forces are distinctly visible on the distal link even in the short time interval, however, the changes are less prominent on the other links – this is reasoned to be due to energy minimization effect.

From Fig. 8 and Fig. 9, it is clear that the drag forces direction on link 1 (base first link) always act in one direction while on link 2 and link 3 the drag force directions vary according to the absolute motion directions and velocity component

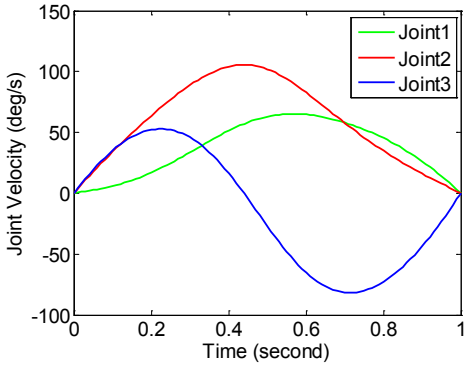

Fig. 6. Joint angular velocities corresponding to minimum energy motion planning

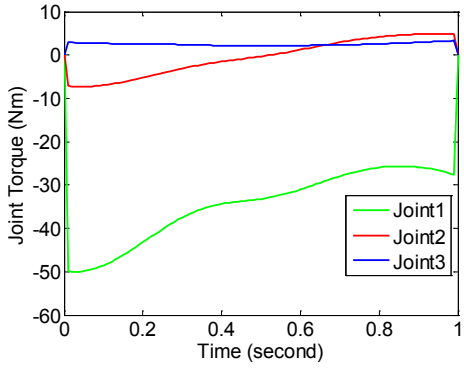

Fig. 7. Joints torque corresponding to minimum energy motion planning

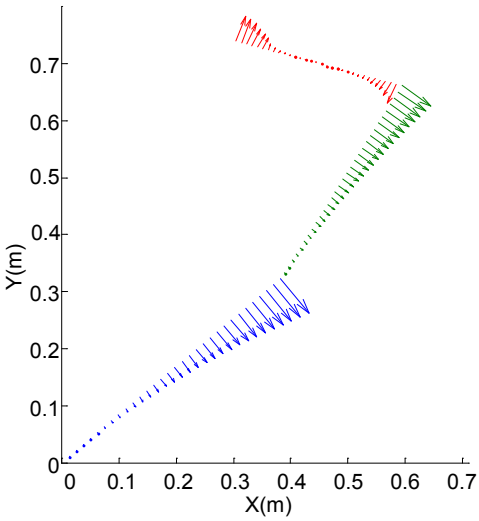

Fig. 8. Drag force distributions on links corresponding to minimum energy at 0.4 s. The blue, green and red arrows represent the pressure drag on link-1, link-2 and link-3 respectively

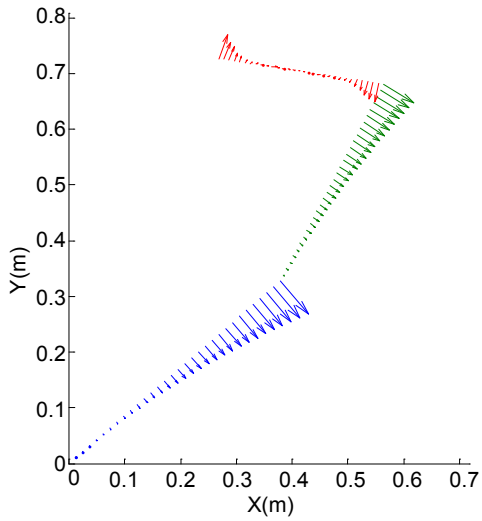

Fig. 9. Drag force distributions on links corresponding to minimum energy at 0.5 s

perpendicular to the links. It is apparent that situations may arrive where drag force may aid in lowering net power consumption and thus motion planning may be suitably carried out utilizing these possibilities.

Fig. 10 shows the net velocities acting on strips of the links in global frame at time step 0.75 s while Fig. 11 shows the pressure drags acting on strips perpendicular to the links. Although the resultant velocities (as shown in Fig. 10) show continuity from link to link, due to different instantaneous link configurations, the normal components show discontinuity, as shown in Fig. 11. Other non-significant

contribution to total drag (including drift and skin effects) are neglected in the present study.

Fig. 12 shows the instantaneous power requirement at different instant of motion to overcome only the hydrodynamic drag for different non-optimal and

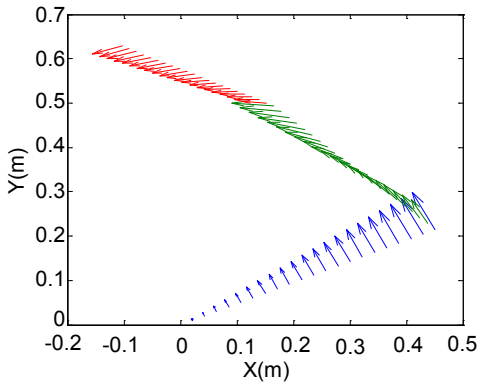

Fig. 10. Net velocity acting on different strips on each link expressed in base frame. The blue, green and red arrows represent the net velocity on link-1, link-2 and link-3 respectively. The length of the arrow indicates magnitudes of the velocities (proportionality represented only)

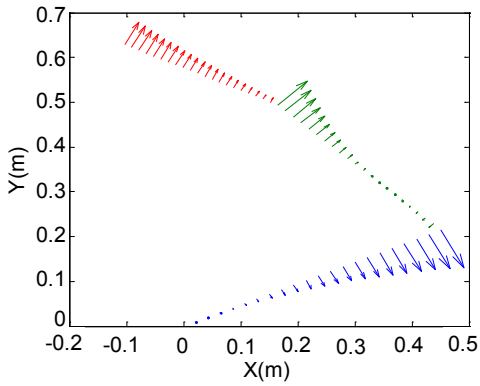

Fig. 11. Pressure drag forces acting on different strips on each links. The blue , green and red colours arrow represent the drag forces on link-1, link-2 and link-3 respectively

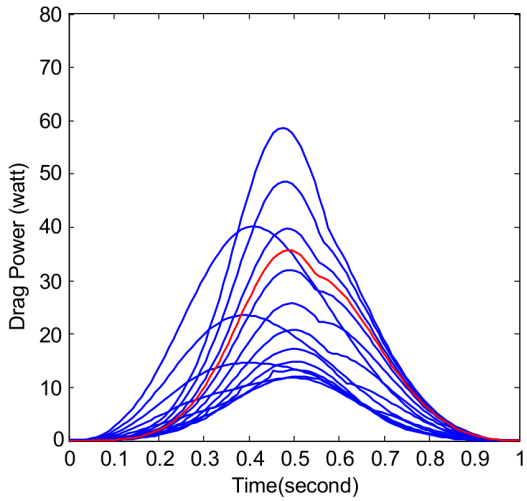

Fig. 12. Instantaneous power requirement, overcoming only hydrodynamic drag force for various non-optimal motions and minimum-energy motion. The blue solid lines are drag power corresponding to non-optimal energies while red solid line is corresponding to the minimum total energy trajectory

minimum-energy motions. The red solid line represents the drag power corresponding to the minimum total energy trajectory and blue solid lines correspond to non-optimal energy trajectory. Similarly, Fig. 13 shows the power curve due to the added mass effect during the motion. From the results it is inferred that energy required in overcoming the hydrodynamic drag forces alone or added mass forces alone are not necessarily the minimum for the minimum total energy trajectory.

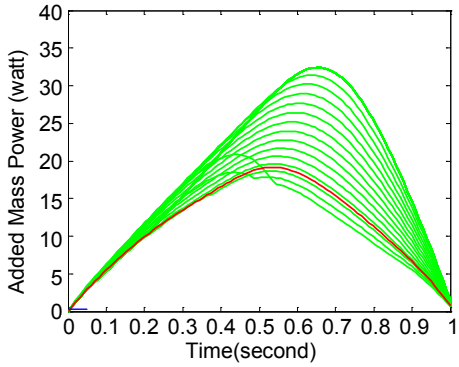

Fig. 13. Instantaneous power requirement for overcoming only hydrodynamic added inertia force. The solid green lines are added mass power corresponding to non optimal energy and red solid line is added mass power, corresponding to the minimum total energy trajectory

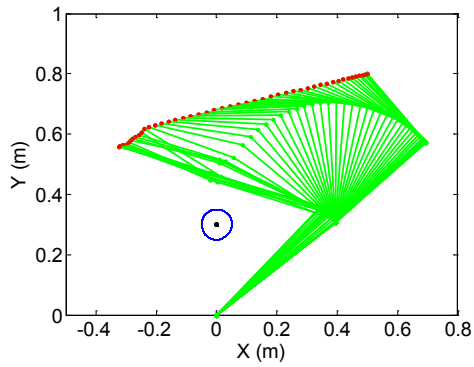

Fig. 14. Series of configuration corresponding to minimum energy motion planning when the singularity avoidance is not considered, however, obstacle avoidance is in force

Figs. 14 and 15 depict with the case, when singularity avoidance is not invoked – it shows the effect of not considering the singularity check. It is accomplished by assigning negligible values to the weighting matrix $\mathbf{W}_v$ (refer to Eq. (18)). Fig. 14 shows the configurations, whereas Fig. 15 plots the joint angular velocity demands. It is apparent and natural that velocity demands become high near the singular configurations, which arise near the end of trajectory in the chosen simulation.

Another case is studied where obstacle avoidance is not considered (see Fig. 16). The corresponding weighting matrix $\mathbf{W}_c$ in Eq. (18) assumes negligible values. The result (series of configurations) is shown in Fig. 16. It is clear that the manipulator links penetrate the safe-circle around the obstacle when the obstacle avoidance criterion is not considered in the motion planning algorithm.

Table 1 presents contributions of energy requirements in overcoming drag forces and added inertia forces for different trajectories, total time spanning 1.2 s, 1.5 s, 2.0 s and 2.5 s for the motion task considered in the exemplar simulation for minimum energy trajectory. For high velocities the hydrodynamic drag plays a dominant role being proportional to cube of velocity and drag also exhibits large variation all along the trajectory.

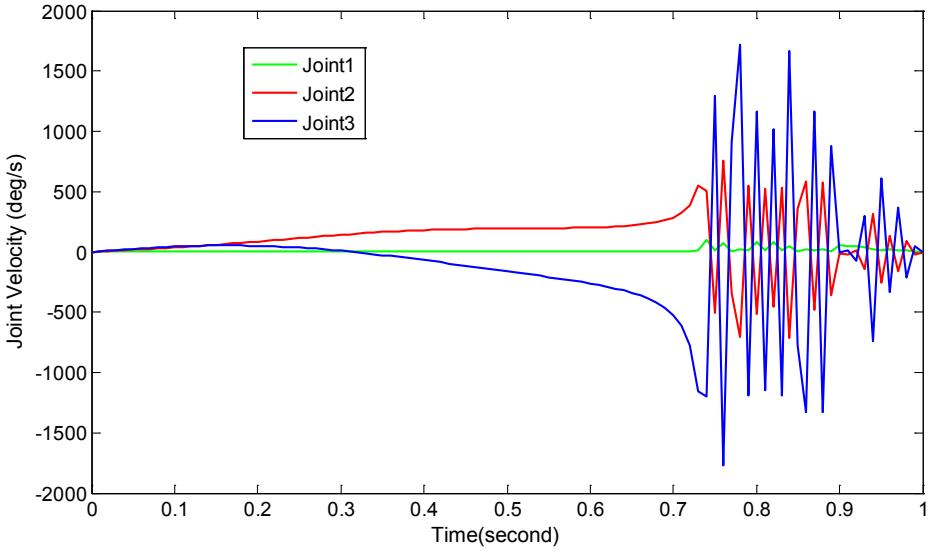

Fig. 15. Joint angular velocity corresponding to minimum energy motion planning when the singularity avoidance is not considered, however, obstacle avoidance is in force

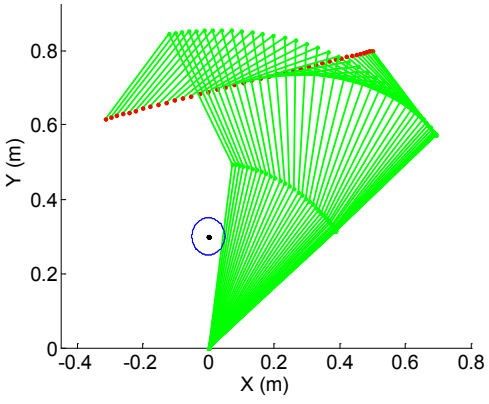

Fig. 16. Series of manipulator configuration when the obstacle avoidance criterion is not considered during the motion planning of manipulator

Table 1.
Drag and Added mass energy contribution in trajectory planning for different total time durations

Total Trajectory Time (s)	Drag Energy Contribution (%)	Added Mass Energy Contribution (%)
1.0	43.39	41.27
1.2	24.3	40.9
1.5	10.1	43.4
2.0	5.51	54.1
2.5	3.2	52.3

7. Conclusions

This article presents the motion planning for redundant serial link underwater manipulator with revolute joints. The motion planning method, for fully submerged manipulator, is based on minimization of total energy spent in overcoming hydrodynamic and dynamic forces. The presented algorithm includes measures for obstacle and singularity avoidances. In order to present the principle of the motion planning method, without loss of much generality, this article considers only a planar manipulator, moving in a vertical plane underwater and under gravity. Hence, all the formulations for kinematics and dynamics computations are derived for the planar application only. The use of standard empirical formulations for hydrodynamics forces of interactions (namely, added inertia force/ torque, drag forces and buoyancy forces) from standard literature enables us to cast the problem from fluid mechanics domain to rigid body mechanics framework. Thus, a recursive Lagrangian dynamics formulation is derived for the underwater planar serial link manipulator with revolute joints to evaluate the joint torque. These torque values are used to evaluate the instantaneous power and total energy during execution of a given task. The developed trajectory planning algorithm is applied in a simulation study, considering a fully submerged underwater manipulator of planar configuration having three degrees-of-freedom and moving in a vertical plane. The formulated optimization algorithm has an inbuilt capacity to take care of avoidance of singularity as well as point obstacle. Simulation of a line following task by the said manipulator is carried out and the results are studied in detail to demonstrate the effectiveness of the proposed motion planning procedure, vis-à-vis the individual effects, namely drag power and added inertia power. The immediate future work will be devoted to extend the algorithm for spatial manipulator, fully or partially submerged underwater. Consideration for multiple and moving underwater obstacles will also be included in the motion planning algorithm, followed by experimental validation of the presented method on an underwater redundant manipulator.

Acknowledgements

This work has been carried out under the activity of the project number MLP-223512 in CSIR-CMERI, Durgapur, a project funded by Council of Scientific and Industrial Research, Govt. of India.

Manuscript received by Editorial Board, January 04, 2021;
final version, September 03, 2021.

References

[1] D.E. Whitney. Resolved motion rate control of manipulators and human prostheses. *IEEE Transaction on Man-Machine System*, 10(2):47–53,1969. doi: 10.1109/TMMS.1969.299896.

[2] Z. Shiller and H-H. Lu. Computation of path constrained time optimal motions with dynamic singularities. *Journal of Dynamic Systems, Measurement, and Control*, 114(1):34–40,1992. doi: 10.1115/1.2896505.

[3] N. Faiz and S.K. Agrawal.Trajectory planning of robots with dynamics and inequalities. In *Proceedings IEEE International Conference on Robotics and Automation*, pages 3976–3982, 2000. doi: 10.1109/ROBOT.2000.845351.

[4] S. Macfarlane and E.A. Croft. Jerk-bounded manipulator trajectory planning: design for real-time applications. *IEEE Transactions on Robotics and Automation*, 19(1):42–52, 2003. doi: 10.1109/TRA.2002.807548.

[5] G. Antonelli, S. Chiaverini, and N. Sarkar. External force control for underwater vehicle-manipulator systems. *IEEE Transactions on Robotics and Automation*, 17(6):931–938, 2001. doi: 10.1109/70.976027.

[6] D. Yoerger and J. Slotine. Robust trajectory control of underwater vehicles. *IEEE Journal of Oceanic Engineering*, 10(4):462–470, 1985. doi: 10.1109/JOE.1985.1145131.

[7] A. Alvarez, A. Caiti, and R. Onken. Evolutionary path planning for autonomous underwater vehicles in a variable ocean. *IEEE Journal of Oceanic Engineering*, 29(2):418–429, 2004. doi: 10.1109/JOE.2004.827837.

[8] N. Sarkar and T.K. Podder. Coordinated motion planning and control of autonomous underwater vehicle-manipulator systems subject to drag optimization. *IEEE Journal of Oceanic Engineering*, 26(2):228–239, 2001. doi: 10.1109/48.922789.

[9] J. Yuh. Modeling and control of underwater robotic vehicles. *IEEE Transactions on Systems, Man and Cybernetics*, 20(6):1475–1483, 1990. doi: 10.1109/21.61218.

[10] B. Lévesque and M.J. Richard. Dynamic analysis of a manipulator in a fluid environment. *International Journal of Robotics Research*, 13(3):221–231, 1994. doi: 10.1177/027836499401300304.

[11] T.I. Fossen. *Guidance and Control of Ocean Vehicles*. John Wiley, New York, 1994.

[12] G. Antonelli. *Underwater Robots*. 2nd ed. Springer, 2006.

[13] T.J. Tarn, G.A. Shoults, and S.P. Yang. A dynamic model of an underwater vehicle with a robotic manipulator using Kane's method. *Autonomous Robots*, 3:269–283, 1996. doi: 10.1007/BF00141159.

[14] J.M. Hollerbach. A recursive Lagrangian formulation of manipulator dynamics and a comparative study of dynamics formulation complexity. *IEEE Transactions on Systems, Man, and Cybernetics*, 10(11):730–736, 1980. doi: 10.1109/TSMC.1980.4308393.

[15] J.N. Newman. *Marine Hydrodynamics. 40th Anniversary Edition*. The MIT Press, 2018.

[16] A. Kumar, V. Kumar, and S. Sen. Dynamics of underwater manipulator: a recursive Lagrangian formulation. In R. Kumar, V.S. Chauhan, M. Talha, H. Pathak (Eds.), *Machines, Mechanism and Robotics*, Lecture Notes in Mechanical Engineering, pages 555–570. Springer, Singapure, 2022. doi: 10.1007/978-981-16-0550-5_56.

[17] A.K. Sharma and S.K. Saha. Simplified drag modeling for the dynamics of an underwater manipulator. *IEEE Journal of Ocean Engineering*, 46(1):40–55, 2021. doi: 10.1109/JOE.2019.2948412.

[18] R. Colbaugh, H. Seraji, and K.L. Glass. Obstacle avoidance for redundant robots using configuration control. Journal of Robotics Systems, 6(6):721–744,1989. doi: 10.1002/rob.4620060605.